Description of large angle ^{6}Li + ^{40}Ca scattering from 26 to 34 MeV using double-folded and $\alpha+d$ cluster potentials

J. Cook, K. W. Kemper, and M. F. Vineyard
Department of Physics, Florida State University, Tallahassee, Florida 32306
(Received 23 April 1982)

New elastic scattering data are reported for ^{6}Li + ^{40}Ca at 26 and 30 MeV, and inelastic data at 30 MeV. The measurements at 30 MeV were taken to provide a complete angular distribution at this energy and showed that previously published large angle data at 30 MeV are incorrectly normalized and must be multiplied by 0.65. The new angular distribution at 26 MeV displays enhanced large angle cross sections as has also been previously observed at 30 and 34 MeV. Double-folded or cluster potentials are able to describe the elastic scattering of ^{6}Li + ^{40}Ca over the energy range 26–34 MeV, including the large angle oscillations. No special property is required to explain the large angle behavior other than weak absorption. The double-folding model has also been used to determine deformation lengths for the first 2^+, 3^-, and 5^- states in ^{40}Ca. The values for the 2^+ and 3^- states agree well with those found from electron, ^{9}Be and ^{11}B inelastic scattering, while the value for the 5^- state is a factor of 2 smaller.

[NUCLEAR REACTIONS ^{40}Ca(^{6}Li,^{6}Li)^{40}Ca, $E=26$ MeV, $\theta_{c.m.}=9°-161°$; ^{40}Ca(^{6}Li, ^{6}Li)^{40}Ca* elastic and 3^-, 2^+, 5^- $E=30$ MeV, $\theta_{c.m.}=9°-78°$; measured $\sigma(\theta)$. Double-folding model, cluster folding model, deduced optical model parameters; DWBA, deduced deformation lengths at 30 MeV.]

I. INTRODUCTION

Recent experimental results[1–3] show that the scattering of ^{6}Li by targets around mass 40 displays enhanced large angle cross sections reminiscent of that observed for α-particle scattering from these same target nuclei. A natural assumption is that the ^{6}Li large angle scattering arises from the underlying α-particle component of an $\alpha+d$ cluster structure in ^{6}Li. Studies of this phenomenon for ^{6}Li have been hampered by the much smaller cross sections ($\sim 10\ \mu$b sr^{-1}) compared with those for the equivalent energy α-particle scattering. The present work reports the results of some new experimental data and analyzes this together with existing data using folded potentials. The new data consist of a complete angular distribution for ^{6}Li+^{40}Ca elastic scattering at 26 MeV, and the forward angle data at 30 MeV necessary to provide a complete angular distribution when combined with the existing data[2] at this energy. In addition, inelastic scattering to the first 2^+, 3^-, and 5^- states in ^{40}Ca has been measured and compared with DWBA calculations.

The elastic data have been analyzed with a microscopic double-folded real potential obtained by convoluting a realistic nucleon-nucleon interaction with the ground state densities of ^{6}Li and ^{40}Ca. This model has previously[4] been applied to the old 28, 30, and 34 MeV data, and was able to describe the data well. However, a discrepancy arose in that different imaginary parameters were required at 30 MeV. With the new 26 and 30 MeV data we wish to try to resolve this discrepancy.

In an attempt to relate the large angle behavior of ^{6}Li+^{40}Ca to that of $\alpha+^{40}$Ca, single-folding cluster potentials have been calculated for ^{6}Li+^{40}Ca assuming that ^{6}Li has an $\alpha+d$ structure. The method used is to fold phenomenological $\alpha+^{40}$Ca and $d+^{40}$Ca potentials with the wave function for $\alpha+d$ in ^{6}Li, and was first described by Watson[5] for ^{6}Li scattering at 20 MeV. It has also been used successfully by Schwandt *et al.*[6] at 99 MeV and in both cases it was found necessary to reduce the strength of the real potential (as also is required for the double-folded potentials) and to use a Woods-Saxon (WS) form for the imaginary potential rather than the cluster form. The $\alpha+d$ cluster model is also

rather successful in describing the vector analyzing power iT_{11} of ^{6}Li scattering around 20 MeV.[6]

II. EXPERIMENTAL PROCEDURE

The ^{6}Li beams for these measurements were produced in an inverted sputter source and accelerated by the Florida State University super FN tandem Van de Graaff accelerator. The targets were made by evaporating natural calcium metal (96.8% ^{40}Ca) onto formvar backings and transferring them under vacuum into the scattering chamber. The forward angle data were taken with a single counter, while the data for $\theta_L > 50°$ were taken with two $\Delta E \times E$ counter telescopes. The counter telescopes were necessary to separate the ^{6}Li events from the larger number of α particles produced. The telescope events were sorted on line so that ^{6}Li energy spectra were produced during the experimental run.

The first data taken were at 30 MeV, where Bohn *et al.*[2] had measured detailed angular distributions for $\theta_L > 40°$. To complete the angular distribution a single detector was used to overlap several data points of Ref. 2 and then the same detector was used to measure the important forward angle Coulomb-nuclear interference region. When these measurements were carried out, they resulted in a cross section that rose to 1.70 of Rutherford, indicating that the data of Ref. 2 were improperly normalized. The slope of the overlap points between the present measurements and those of Ref. 2 was the same. Several data points were taken at 28 and 34 MeV to normalize the 30 MeV data to those of Ref. 1, where considerable effort was made to determine the absolute cross section. Our results show that the data of Ref. 2 need to be multiplied by 0.65 to give them the proper normalization. A previous study[12] which analyzed ^{6}Li+^{40}Ca elastic scattering in a consistent manner over the energy range 28—156 MeV using a single energy independent potential had found a normalization of 0.70 for the 30 MeV data of Ref. 2. A combination of the present results with those of Ref. 2 after they have been multiplied by 0.65 is presented in Fig. 1. The data taken in the present work at 26 MeV are also shown in Fig. 1 and the inelastic data at 30 MeV are presented in Fig. 4. The absolute error of all the data shown is $\pm 7\%$. The sources of this error are discussed in Ref. 1. The error bars in the figures represent the sum of statistical errors and peak fitting errors. Minimum relative errors of 5% were assumed at all energies.

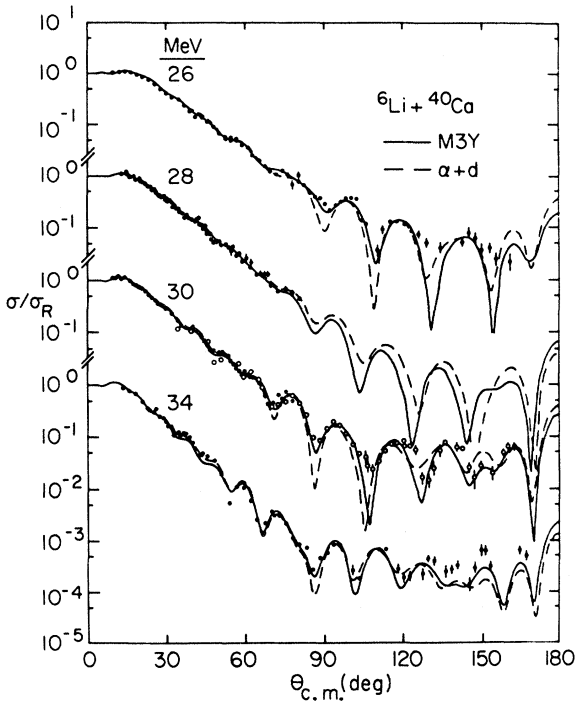

FIG. 1. Fits to ^{6}Li+^{40}Ca elastic scattering at 26—34 MeV using real potentials obtained by a double folding of the $M3Y$ interaction with the densities of ^{6}Li and ^{40}Ca ($M3Y$, full lines), or by a superposition of α and deuteron potentials ($\alpha+d$, dashed lines). The imaginary potential had a Woods-Saxon form in both cases. The data of Ref. 2 after multiplication by 0.65 are shown as open circles.

III. ELASTIC SCATTERING

Previously published analyses[1,2] of ^{6}Li +^{40}Ca elastic scattering at 30 and 34 MeV using Woods-Saxon potentials have been unable to fit the so-called anomalous large angle ($\theta \geq 90°$) data. In contrast, the double-folding model[4] is able to satisfactorily describe the large angle data at 30 MeV, although the forward angle data is lacking at this energy. This model is applied here to 26—34 MeV data over the angular range 10°—170°.

The real potential $V_F(r)$ is calculated by folding an effective nucleon-nucleon interaction $v(r)$ with the densities of both the projectile $\rho_p(r)$ and target $\rho_T(r)$

$$V_F(\vec{r}) = \int d\vec{r}_p \int d\vec{r}_T \rho_p(\vec{r}_p) \times \rho_T(\vec{r}_T) v(\vec{r} - \vec{r}_p + \vec{r}_T) \,. \quad (1)$$

The effective interaction is taken to be the $S=T=0$ component of the $M3Y$ interaction determined by Bertsch *et al.*,[7] modified by inclusion of a

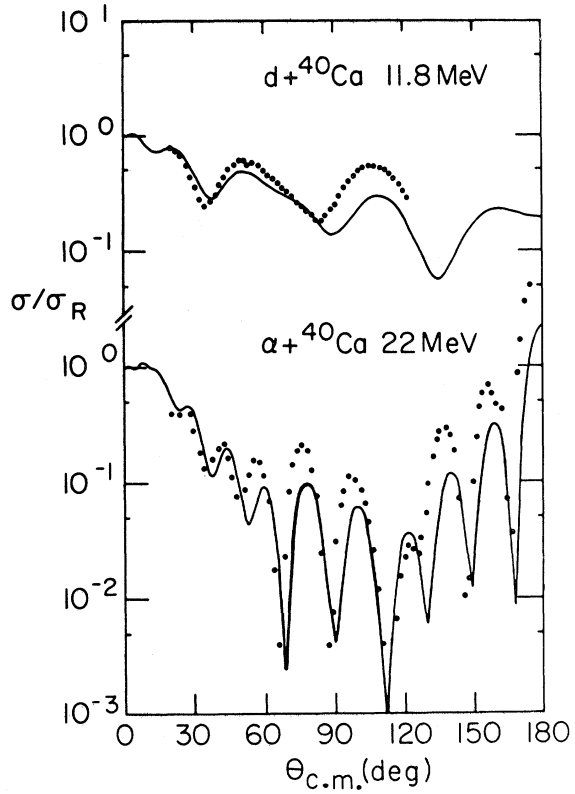

FIG. 2. Optical model predictions for the elastic scattering of $d+^{40}$Ca at 11.8 MeV and $\alpha+^{40}$Ca at 22 MeV. The data are from Refs. 17 and 18, and the optical potentials from Refs. 15 and 16.

delta function to account for single nucleon exchange

$$v(r)=7999\frac{e^{-4r}}{4r}-2134\frac{e^{-2.5r}}{2.5r}-262\delta(r)\ . \quad (2)$$

For the ^{6}Li projectile density, the proton charge distribution was unfolded from the measured charge density[8] and it was assumed that neutron and proton densities were equal. A semi-self-consistent calculation with a density dependent potential was used to generate the ^{40}Ca density.[9] The folded potential was then calculated with the computer program DFPOT[10] using standard Fourier transform techniques.

The folded potential was multiplied by a normalization factor N to compensate for deficiencies in the model. Since the interaction used was real and there is no reason to suppose that the real and imaginary parts of the interaction have the same form, an imaginary Woods-Saxon potential was used

$$W(r)=-iW_0\left[1+\exp\left[\frac{r-r_I A_T^{1/3}}{a_I}\right]\right]^{-1}\ . \quad (3)$$

TABLE I. Optical model parameters for ^{6}Li+^{40}Ca elastic scattering at 26–34 MeV.

E (MeV)	N	W_0 (MeV)	r_I (fm)	a_I (fm)
	Double-folded real potentials			
26	0.65	9.63	1.99	0.69
28	0.65	11.24	1.98	0.75
30	0.63	10.01	1.97	0.68
34	0.64	11.06	1.94	0.73
	$\alpha+d$ real potentials			
26	0.61	7.76	2.03	0.84
28	0.62	10.18	1.97	0.88
30	0.60	8.78	1.96	0.81
34	0.59	10.01	1.94	0.82

In fact, using the same folded form for both real and imaginary potentials does not fit the data. Also included was the Coulomb potential due to a uniformly charged sphere of radius $R_C=1.3A_T^{1/3}$ fm. The optical model program FBOMP[11] was used to search on the parameters to fit the data. The resulting parameters are given in Table I and the fits are shown as the full lines in Fig. 1. The fits are very good over the whole angular range of the data at each energy. In particular they are able to describe the deep large angle oscillations while simultaneously fitting the forward angle data, which was not demonstrated convincingly in Ref. 4.

Satchler and Love[4] also fitted the old 28, 30, and 34 MeV data with the double-folded potential and noticed a discrepancy in that the 30 MeV data required smaller values for W_0 and a_I compared with the neighboring energies of 28 and 34 MeV, while N and r_I were consistently the same at all three energies. Since changes in the normalization of the data can be compensated for by different imaginary potentials, we thought that the discrepancy might therefore arise from an incorrect normalization of the 30 MeV data, or from a lack of forward angle data. However, even when the 30 MeV data are correctly normalized and the forward angles included, the discrepancy still remains, as can be judged from the parameters in Table I. We do find, however, that the discrepancy is not as serious as with the incorrectly normalized data, for which we obtained the parameters $N=0.63$, $W_0=9.51$ MeV, $r_I=2.03$ fm, and $a_I=0.59$ fm. Moreover, the 26 MeV imaginary parameters are very similar to those at 30 MeV and therefore exhibit the same discrepancy. Since the normalization of the data at each energy has been carefully determined, it would appear that there are small fluctuations in the ima-

ginary parameters in this energy range, although for higher energies up to 156 MeV the ^{6}Li+^{40}Ca potential is energy independent.[12] Another point to note is that to fit the large angle data at energies around 30 MeV the imaginary radius parameter $r_I \approx 2.0$ fm is much larger than the value $r_I \approx 1.7$ fm required to fit high energy data. Accompanied with this are smaller values of W_0 at low energies. However, there still is no variation in the real potential with increasing energy.

Calculations have also been made using a superposition of alpha and deuteron potentials to see if the anomalous large angle scattering observed for ^{6}Li is related to that for the scattering of alpha particles from ^{40}Ca. The real potential for ^{6}Li is calculated from

$$V_{^6\mathrm{Li}}(r)=\int \{ V_\alpha(\vec{r}-\tfrac{1}{3}\vec{R}) + V_d(\vec{r}+\tfrac{2}{3}\vec{R})\} \, |\psi(\vec{R})|^2 d\vec{R} \, , \quad (4)$$

where $V_\alpha(r)$ and $V_d(r)$ are the real parts of the alpha and deuteron optical potentials, evaluated at $\frac{2}{3}$ and $\frac{1}{3}$ of the incident ^{6}Li energy. $\psi(R)$ is the wave function of relative motion for the alpha and deuteron clusters within ^{6}Li and is taken from the work of Kurdyumov *et al.*[13] It is found, however, that the resulting ^{6}Li potential is very insensitive to the exact form of the $\alpha-d$ wave function and that almost identical results are obtained using different[9,14] wave functions.

The alpha and deuteron real potentials have the form of a Woods-Saxon potential raised to a power

$$V_{\alpha(d)}(r) = -V_{\alpha(d),0}\left[1+\exp\left[\frac{r-r_{\alpha(d)}A_T^{1/3}}{a_{\alpha(d)}}\right]\right]^{-N_{\alpha(d)}} , \quad (5)$$

where the global parameters of Daehnick *et al.*[15] are used for the deuteron potential

$$\begin{aligned} V_{d,0}&=93.6-0.26E \, , \\ r_d&=1.17 \, , \\ a_d&=0.709-0.0017E \, , \\ N_d&=1 \, , \end{aligned} \quad (6)$$

and the average parameters of Gubler *et al.*[16] for $\alpha+^{40}$Ca are used for the alpha potential

$$\begin{aligned} V_{\alpha,0}&=241.0-0.279E \, , \\ r_\alpha&=1.88 \, , \\ a_\alpha&=1.85 \, , \\ N_\alpha&=5 \, . \end{aligned} \quad (7)$$

The ^{6}Li energies of this work correspond to deuteron energies of 7.7–10.1 MeV and alpha-particle energies of 16.6–21.7 MeV. The global deuteron potential of Ref. 16 was obtained from fitting data in excess of 11.8 MeV. Figure 2 shows a fit to $d+^{40}$Ca data at 11.8 MeV from Ref. 17 using the global deuteron potential. It is claimed in Ref. 16 that the difference between data and theory at large angles is due to contributions from *s*-wave compound elastic scattering. However, the data may be fitted well at all angles by only small departures from the global parameters. It is therefore expected that the use of the global potential is reasonable.

The $\alpha+^{40}$Ca potential of Gubler *et al.*,[16] with a WS (Ref. 5) shape for the real part and a WS shape for the imaginary part, is capable of fitting data over the energy range 29–104 MeV, including the large angle behavior at the lower energies, remarkably well. However, it fails when applied to lower energy data, such as the 22 MeV data of Ref. 18 shown in Figure 2. It is capable of predicting the correct general shape, but the magnitudes of the peaks are too low for $\theta \geq 50°$ by a factor of about 2. Searching on the parameter values is unable to significantly improve the fit, nor is the use of other $\alpha+^{40}$Ca potentials which are able to fit higher energy data. We note here that improvements in the description of the large angle data appear to come from changes in the shape of the imaginary poten-

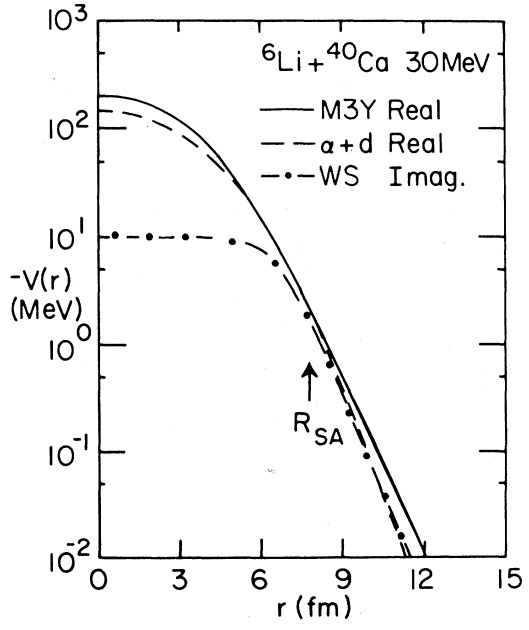

FIG. 3. Real and imaginary potentials for ^{6}Li+^{40}Ca elastic scattering at 30 MeV. The strong absorption radius is marked as R_{sa}.

tial and therefore justify the use of Eqs. (5) and (7) for calculating the alpha component of the ^{6}Li real potential.

The ^{6}Li+^{40}Ca elastic data was then refitted using the $\alpha+d$ potential. As before the real potential was multiplied by a normalization factor N and a volume Woods-Saxon potential included. The superposition model cannot be expected to yield a realistic imaginary potential due to the different absorptive mechanisms involved. In particular it will omit the breakup channel of ^{6}Li into $\alpha+d$, which is likely to be large. The resulting parameters are given in Table I and the fits are shown as the dashed lines in Fig. 1. The fits to the data are again quite good over the whole angular range, although the χ^2 values are about twice as large as when using the double-folded potential.

Comparing the parameters for the two different potential forms, the double-folded potential has an average normalization of $\bar{N}=0.64$ and the $\alpha+d$ potential one of $\bar{N}=0.61$. The difference between these values is not very significant. However, the folded potential has an average volume integral per interacting nucleon of 261 MeV fm^3, while that for the $\alpha+d$ potential is 224 MeV fm^3. The discrepancy can be traced to the $\alpha+^{40}$Ca potential which has a volume integral per interacting nucleon of about 350 MeV fm^3 compared with 405 MeV fm^3 for the deuteron potential and 408 MeV for the nucleon-nucleon interaction of Eq. (2). There is little difference between the imaginary potentials, although the diffuseness is consistently larger for the $\alpha+d$ fits.

Figure 3 illustrates the different potentials at 30 MeV. The folded ($M3Y$) and $\alpha+d$ real potentials are very similar for $r=5-8$ fm, but the $\alpha+d$ potential is smaller in magnitude outside this region. However, the important point to note is that the imaginary potential is always smaller than both real potentials for $r\leq 10$ fm, in particular at the strong absorption radius $R_{sa}=1.5(6^{1/3}+40^{1/3})$ fm. This is one of the few cases in ^{6}Li scattering where the imaginary potential is not dominant at large radii. The weaker absorption, presumably arising from a reduced number of open reaction channels, then gives rise to the large angle oscillations in exactly the same way as for $\alpha+^{40}$Ca.[25]

IV. INELASTIC SCATTERING

Simultaneously with the forward angle elastic data at 30 MeV, inelastic cross sections for the excitation of the first 2^+, 3^-, and 5^- states in ^{40}Ca were measured. These data have been analyzed in the same way as previously used for excitation of the same states by ^{9}Be (Ref. 19) and ^{11}B (Ref. 20) inelastic scattering to determine if the deformation lengths are consistent.

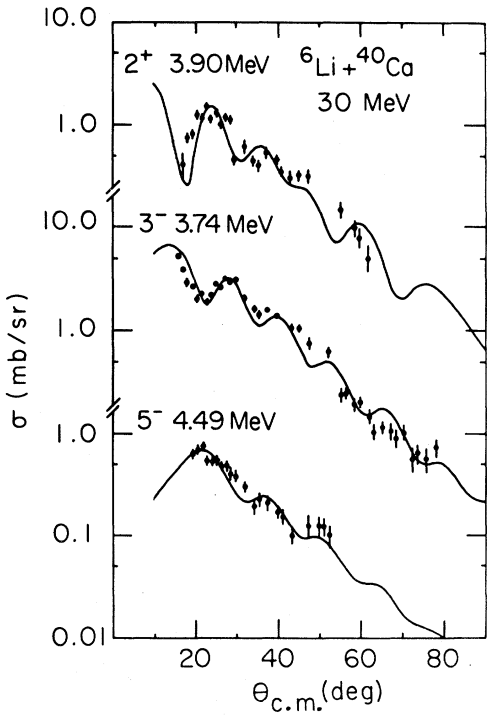

FIG. 4. DWBA calculations of ^{6}Li+^{40}Ca inelastic scattering at 30 MeV using realistic transition densities to calculate the real form factors in a double folding model.

Since the previous papers for ^{9}Be and ^{11}B used a different density distribution for ^{40}Ca, the elastic data was first refitted. The form of the ^{40}Ca density was taken from the liquid drop model[21]

$$\rho_T(r)=\frac{0.0849}{1+\exp\left[\frac{r-3.572}{0.55}\right]}+\frac{0.0858}{1+\exp\left[\frac{r-3.558}{0.55}\right]} \quad (8)$$

and the proton charge was unfolded. The same density as before was used for ^{6}Li. The single nucleon exchange strength was now taken as 390 MeV fm^3 to maintain consistency. The 30 MeV elastic scattering data is then fitted with the parameters $N=0.67$, $W_0=12.41$ MeV, $r_I=1.92$ fm, and $a_I=0.66$ fm with very similar fits to those obtained in the previous section.

It was assumed that a derivative form could be used for the 2^L-pole transition densities $\rho_L(r)$

TABLE II. Deformation lengths for inelastic transitions in ^{40}Ca.

Transition	Q (MeV)	L	B(EL) (e^2fm^{2L})	δ_L[a](EL) (fm)	δ_L(^{6}Li)[b] (fm)	δ_L(^{9}Be)[c] (fm)	δ_L(^{11}B)[d] (fm)
$0^+\rightarrow 2^+$	−3.90	2	90[e]	0.46	0.49	0.44	0.44
$0^+\rightarrow 3^-$	−3.74	3	1.5×10^4[e]	1.30	1.04	1.15	1.15
$0^+\rightarrow 5^-$	−4.49	5	3×10^6[f]	0.75	0.53	0.81	1.00

[a]Derived from the B(EL) values using Eq. (10).
[b]Found by fitting the present data.
[c]Reference 19.
[d]Reference 20.
[e]Reference 23.
[f]Reference 24.

$$\rho_L(r)=\delta_L\frac{d\rho_0}{dr}\ , \tag{9}$$

where $\rho_0(r)$ is the spherical density for ^{40}Ca given by Eq. (8). δ_L is the 2^L-pole nuclear deformation length for the inelastic transition. The imaginary part of the transition form factor had the normal Woods-Saxon derivative form with the same deformation parameter as used for the real part. The inelastic cross sections were calculated in the DWBA using the computer program CHUCK3.[22] The distorted waves were generated with the renormalized double-folded real and Woods-Saxon imaginary potentials which fitted the elastic data. The same renormalization was used for the real double-folded inelastic form factors. Coulomb excitation was included and the deformation lengths δ_L were adjusted to fit the magnitude of the inelastic cross sections.

The resulting deformation lengths are compared in Table II with those found from folding model analyses of ^{9}Be and ^{11}B inelastic scattering. A deformation length for the charge distribution may also be derived from the reduced electric transition probability $B(\mathrm{EL};0\rightarrow L)$ by

$$\int_0^\infty \rho_L(r)r^{L+2}dr=\frac{A}{Ze}[B(\mathrm{EL})]^{1/2} \tag{10}$$

and is also given in Table II. The deformation lengths for the 2^+ and 3^- states found from ^{6}Li inelastic scattering agree well with those found from the B(EL) values and from ^{9}Be and ^{11}B inelastic scattering. However, the deformation length for the 5^- state is rather lower for ^{6}Li inelastic scattering than for any of the other methods, although it does agree well with the result found for ^{11}B inelastic scattering[20] using real Woods-Saxon potentials and form factors.

It is possible that the discrepancy in the deformation lengths arises from the greater sensitivity to the real form factors (due to weaker absorption) in the scattering of ^{6}Li from ^{40}Ca compared with ^{9}Be and ^{11}B. Following previous folding model calculations of inelastic scattering[4,26] Tassie transition densities

$$\rho_L(r)=C_L r^{L-1}\frac{d\rho_0}{dr} \tag{11}$$

normalized to the B(EL) values were used to calculate the real form factors. The extra r^{L-1} factor in Eq. (11) compared with Eq. (9) results in a longer tail for the high L values and also the peak in the transition density is located further out in radius as L increases. The deformation lengths of the imaginary form factors were adjusted to fit the data and resulted in $\delta_L=0.74$, 1.30, and 0.61 for the 2^+, 3^-, and 5^- states, respectively. While the deformation length for the 5^- state has increased, it is still somewhat less than the deformation lengths obtained from the B(EL) value, and ^{9}Be and ^{11}B scattering. In addition the 2^+ deformation length is much greater than was previously obtained. It is therefore concluded that the discrepancy in the 5^- deformation length is not attributed to an incorrect choice for the transition densities. It is more likely to be due to an incorrect parametrization of the imaginary potential since even though it appears to be weakly absorbing the real form factors alone produce only about 10−20 % of the inelastic cross section.

V. CONCLUSIONS

New experimental data for ^{6}Li+^{40}Ca elastic scattering at 26 and 30 MeV have been measured. The 26 MeV data, extending to large angles, show enhanced large angle cross sections, as previously observed at 30 and 34 MeV. The new 30 MeV data show that the normalization of previously published large angle data at this energy is in error, and that this data should be multiplied by 0.65 to be consistent with the forward angle data presented here. In addition, inelastic transitions to the first 2^+, 3^-, and 5^- excited states in ^{40}Ca were measured at an incident energy of 30 MeV.

The new elastic data measured here have been

analyzed in conjuction with existing data at 28, 30, and 34 MeV. Both the forward angle data and the enhanced large angle oscillations may be simultaneously fitted using a real potential obtained from either a double-folding calculation or a single-folding cluster model. In contrast to the general case for ^{6}Li, the imaginary potential is required to be weaker than the real at all radii in order to describe the large angle data. The similarity of the double folded and cluster potentials, and the weakness of the imaginary potential, suggest that the large angle behavior of $^6\mathrm{Li}+^{40}\mathrm{Ca}$ is not particularly related to the $\alpha+^{40}$Ca component, but rather is due to the weak absorption in this case.

The inelastic data were compared with DWBA calculations employing double-folded real and phenomenological imaginary form factors. The deformation lengths were adjusted to fit the magnitude of the data and for the 2^+ and 3^- states were found to agree well with the values obtained for inelastic electron, ^{9}Be and ^{11}B scattering. However, the deformation length for the 5^- state was found to be about a factor of 2 smaller.

This work was supported in part by the National Science Foundation.

[1]R. I. Cutler, M. J. Nadworny, and K. W. Kemper, Phys. Rev. C 15, 1318 (1977).
[2]H. Bohn, K. A. Eberhard, R. Vandenbosch, K. G. Bernhardt, R. Bangert, and Y. D. Chan, Phys. Rev. C 16, 665 (1977).
[3]J. Szymakowski, K. W. Kemper, and A. D. Frawley, Nucl. Phys. A355, 221 (1981).
[4]G. R. Satchler and W. G. Love, Phys. Rep. 55, 183 (1979).
[5]J. W. Watson, Nucl. Phys. A198, 129 (1972).
[6]H. Amakawa and K-I Kubo, Nucl. Phys. A266, 521 (1976); W. Weiss, P. Egelhof, K. D. Hildenbrand, D. Kassen, M. Makowska-Rzeszutko, D. Fick, H. Ebinghaus, E. Steffens, A. Amakawa, and K-I Kubo, Phys. Lett. 61B, 237 (1976); P. Schwandt, W. W. Jacobs, M. D. Kaitchuck, P. P. Singh, W. D. Ploughe, F. D. Becchetti, and J. Jänecke, Phys. Rev. C 24, 1522 (1981).
[7]G. Bertsch, J. Borysowicz, J. McManus, and W. G. Love, Nucl. Phys. A284, 399 (1977).
[8]L. R. Suelzle, M. R. Yearian, and H. Crannell, Phys. Rev. 162, 992 (1967).
[9]B. A. Brown, S. E. Massen, and P. E. Hodgson, J. Phys. G 5, 1655 (1979).
[10]J. Cook, Comp. Phys. Commun. 25, 125 (1982).
[11]J. Cook (unpublished).
[12]J. Cook, Nucl. Phys. A375, 238 (1982).
[13]I. V. Kurdyumov, V. G. Neudatchin, Yu. F. Smirnov, and V. P. Korennoy, Phys. Lett. 40B, 607 (1972).
[14]A. K. Jain, J. Y. Grossiord, M. Chevallier, P. Gaillard, A. Guichard, M. Gusakow, and J. R. Pizzi, Nucl. Phys. A216, 519 (1973).
[15]W. W. Daehnick, J. D. Childs, and Z. Vrcelj, Phys. Rev. C 21, 2253 (1980).
[16]H. F. Gubler, U. Kiebele, H. O. Meyer, G. R. Plattner, and I. Sick, Nucl. Phys. A351, 29 (1981).
[17]C. Igo, W. Lorenz, and U. Schmidt-Rohr, Phys. Rev. 124, 832 (1961).
[18]G. Gaul, H. Ludecke, R. Santo, H. Schmeing, and R. Stock, Nucl. Phys. A137, 177 (1969).
[19]V. Hnizdo, J. Szymakowski, K. W. Kemper, and J. D. Fox, Phys. Rev. C 24, 1495 (1981).
[20]V. Hnizdo, C. W. Glover, and K. W. Kemper, Phys. Rev. C 23, 236 (1981).
[21]W. D. Myers, Nucl. Phys. A145, 387 (1970).
[22]P. D. Kunz, University of Colorado (unpublished) with modifications by J. R. Comfort.
[23]P. L. Hallowell, W. Bertozzi, J. Heisenberg, S. Kowalski, X. Maruyama, C. P. Sargent, W. Turchinetz, and C. F. Williamson, Phys. Rev. C 7, 1396 (1973).
[24]J. Heisenberg, J. S. McCarthy, and I. Sick, Nucl. Phys. A164, 353 (1971).
[25]K. A. Eberhard, Phys. Lett. 33B, 343 (1970).
[26]J. Cook, J. Phys. G 7, L67 (1981); G. R. Satchler, Phys. Rev. C 22, 919 (1980).